Formation of Deuterium-Ice Layers in OMEGA Targets

When the OMEGA Cryogenic Target Handling System (CTHS) became operational in July 2000, it was the culmination of a seven-year engineering effort to build the infrastructure needed to produce cryogenic inertial confinement fusion (ICF) targets. These targets are used for implosion experiments that are a one-third scale of the experiments to be performed on the National Ignition Facility (NIF). These experiments allow issues that affect the quality of the implosion, such as the hydrodynamic stability and laser imprint, to be correlated to the laser performance and target specifications.

This article discusses the process of forming a cryogenic target—specifically, how to make a 0.9-mm-diam shell of deuterium ice constrained in a thin-walled plastic shell. The process differs from that developed for earlier cryogenic systems in many aspects: (1) there is sufficient deuterium mass to form thick-walled (100-μm) shells; (2) the deuterium is permeated into the plastic shell, eliminating the need for a filling tube, which can perturb the thermal environment and influences the process; (3) the system possesses all of the engineering features needed to deliver a target for implosion, so the effect of those features are included in the process demonstrated to make cryogenic targets; and (4) the CTHS system can also produce cryogenic NIF-sized targets, which will allow the cryogenic processes to be demonstrated on full-sized ignition targets, even if the targets are too massive to be imploded on OMEGA in meaningful experiments. Schematics of OMEGA- and NIF-scale, direct-drive cryogenic targets are shown in Fig. 99.21. The OMEGA cryogenic target is a 0.9-mm-diam plastic shell with a 3-μm wall that is diffusion filled to a maximum pressure of 1500 atm. This gas density equates to a solid-deuterium wall thickness of up to 130 μm—one-third scale of a NIF direct-drive-ignition target.

Overview of the Process Used to Make Cryogenic Targets

The process of transforming a plastic shell containing liquid deuterium into a cryogenic ICF target where a uniformly thick wall of deuterium ice adjoins the inner plastic wall is referred to as "layering."

Initially, an empty plastic shell is at vacuum and room temperature inside a pressure vessel. A hydrogen-isotope gas (deuterium presently and a deuterium–tritium mixture in the future) is added to the vessel until the pressure is approximately 1000 atm (depending on the desired ice thickness and shell dimensions). For any pressure ramp lower than the ratio of the shell's buckle pressure to the permeation rate (typically 1 atm per minute), the hydrogen gas will diffuse through the plastic without buckling the shell. Once the plastic shell

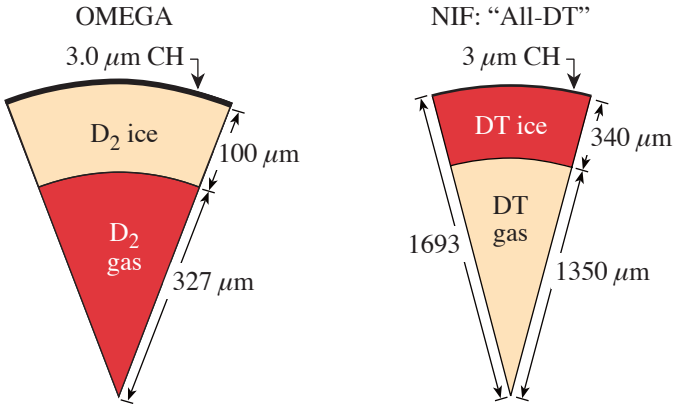

Figure 99.21
Schematic showing the dimensions of direct-drive targets for use on OMEGA and the NIF.

contains sufficiently dense hydrogen gas (~0.1 g/cm^3), it is gradually cooled: the liquid phase first appears at the critical point (38 K) and the solid forms at the triple point (18.72 K). At 18.72 K the hydrogen fuel is a solid "lump" with a vapor pressure of less than 200 Torr. The plastic shell is removed from the pressure vessel and transferred, inside a cryostat, to the mobile cryostat that transports the target to the OMEGA target chamber. The latter cryostat has two critical components: (a) a 2.5-cm-inner-diam isothermal copper shell that is placed around the target and (b) the "life-support" equipment required to sustain the target at all times.

When the target is centered inside the isothermal copper shell (called the *layering sphere*), it is bathed in infrared light at a wavelength that is absorbed by the deuterium. The combination of volumetric heating from the IR light and the isothermal boundary at the layering sphere creates a temperature gradient within the deuterium: the deuterium is warmest where it is thickest and closest to the center of the sphere. In minimizing this temperature gradient, the ice/liquid redistributes itself on the inside surface of the plastic shell. Eventually the ice forms a contiguous shell wall with an isothermal inner surface. The goal is a uniform-thickness deuterium-ice wall with a root-mean-square (rms) thickness variation of less than 1 μm.

The metric for the ice-layer quality is the roughness of the inner surface, which is equated to the ice-wall-thickness uniformity; however, the suitability of this value as a proxy for ice-thickness uniformity depends on the sphericity of the outer deuterium wall and, hence, the plastic shell, which defines the geometry. Typically, a plastic shell possesses an eccentricity of 0.1 μm to 0.5 μm and the wall thickness varies by <0.2 μm—values that can affect the ice-thickness uniformity and cause the ice roughness and thickness uniformity to differ. For a uniformly thick plastic shell with an isothermal outer surface, the ice shell will be uniformly thick if the radial thermal conductance is constant around the target. Under these optimal circumstances, any roughness on the inner surface of the ice will be due to the crystalline structure of the ice. In practice, such higher-spatial-frequency roughness is overwhelmed by low-mode roughness caused by imperfections in the target and asymmetries in the layering sphere.

Four years' experience in producing cryogenic targets identifies the elimination of the low-mode ice roughness as the major challenge to producing high-quality implosion targets. The highest-quality ice layers have an rms roughness of 1.2 μm, averaged over the entire surface (see Fig. 99.22). More typically, the roughness averages 3 μm to 6 μm, although values as great as 8 μm to 10 μm also occur. This article analyzes potential causes for the low-mode roughness and provides experimental data quantifying the effect of the perturbations on the roughness magnitude. Thermal and ray-tracing models make explicit how sensitive the ice roughness is to its environment. This allows a better understanding of the required level of control from the cryogenic equipment and provides better direction for improving the equipment.

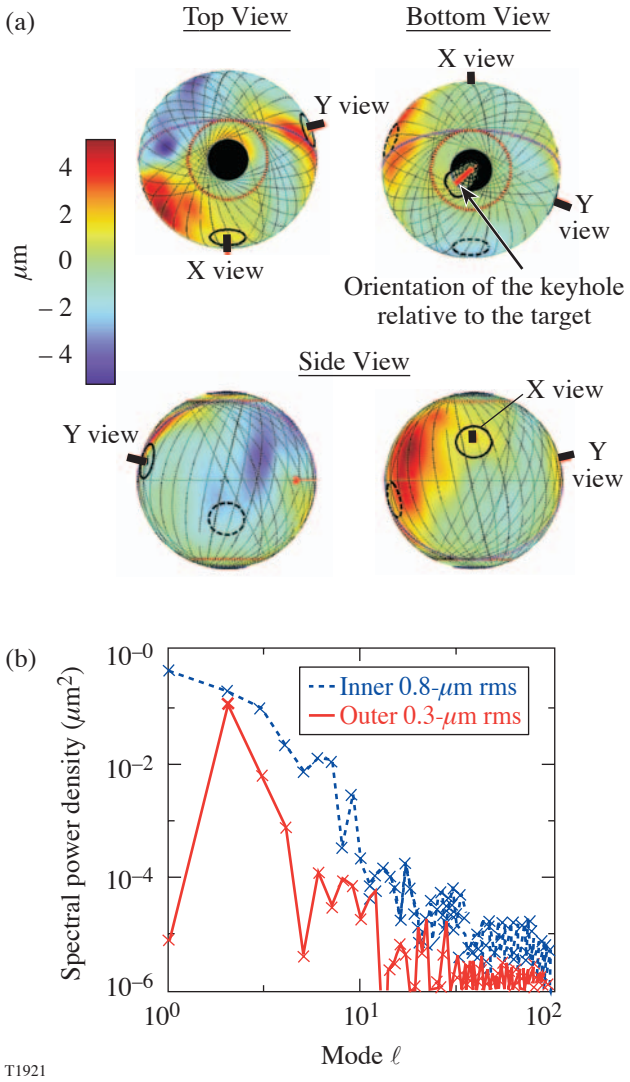

Figure 99.22
(a) Four views of the surface of an 80-μm-thick, 880-μm-diam spherical ice layer. The shading shows the variation in thickness of the ice. The 3-D profile is compiled from 50 2-D views. (b) Two-dimensional power spectra of the inner ice surface and the outer plastic surface.

Introduction

The concept of layering was first demonstrated by radioactively inducing sublimation in solid tritium.[1] Subsequent work at Los Alamos National Laboratory (LANL) and Lawrence Livermore National Laboratory (LLNL) expanded the science and better quantified the process. This work relied on heat generated by the decay of a triton atom yielding a ^{3}He nucleus, a beta electron, and an antineutrino with 18.6 keV of energy collectively. The average β energy is 6 keV and equates to a volumetric heating rate of 51 kW/m^3 (0.977 W/mol, hereafter referenced as 1 Q_{DT}). Subsequent work at LLNL demonstrated that volumetric heating could also be achieved by radiatively heating the hydrogen-isotope ice using infrared illumination.[2] This method made it possible to "layer" nontritium hydrogen isotopes and is used to make the deuterium-ice layers studied and reported here.

An important difference between work reported here and earlier layering work is the geometry of the layering environment and the absence of a fill tube; earlier studies used geometries such as hemispheres, cylinders, and other surrogate geometries. These compromises simplified both filling the targets (a diffusion-filling capability is both complex and expensive) and diagnosing the layering process. However, the fill tube affected the thermal environment around the target, which affects the layering process itself. A protocol for a fill-tube-free layering method, and the resulting layer quality, is presented in the remaining sections, which (1) deal with the principles of the layering process, (2) examine the methodology of experimentally measuring the success of layering, (3) discuss how various parameters affect the layering process, and (4) present a summary and discussion.

Layering Process

Experimentally, the process used to form a layer is straightforward: The target is centered in a 2.5-cm-diam, temperature-controlled, hollow sphere—the layering sphere (Fig. 99.23). The sphere contains helium gas to conduct the heat away from the target. The internal surface of the sphere is purposely roughened to form an "integrating sphere," which allows the target to be uniformly irradiated with infrared light at 3.16 μm, a frequency that corresponds to the strongest absorption band in the deuterium-ice [the $Q_1(1) + S_0(0)$ and $Q_1(0) + S_0(0)$ bands] molecular crystal,[3] in which each crystal-lattice site is occupied by one D_2 molecule.

There are two procedures for layering targets: One process starts with the target below the triple point (18.72 K) and a frozen lump of deuterium in the bottom of the target. Deuterium absorbs the IR light and becomes warmer than the plastic shell's outer surface. Solid deuterium sublimes from where it is thickest (and therefore hottest because of volumetric heating) and condenses where it is thinnest. In theory, the ice wall will become uniformly thick. In practice, there is an ~10- to 20-μm peak-to-valley variation in ice thickness formed by this method.

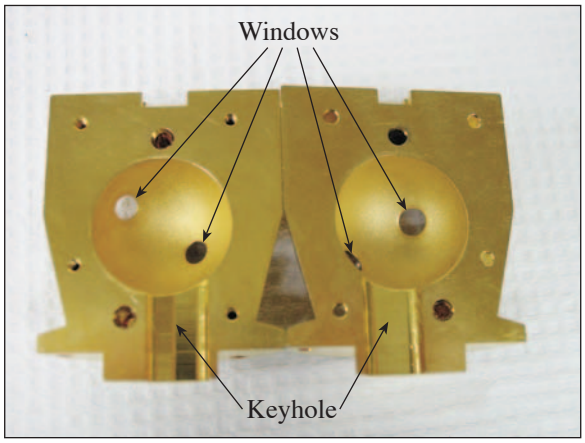

T1933

Figure 99.23
The two hemispheres that comprise the layering sphere are shown side by side. The "keyhole" opening at the base of the layering sphere is where the target is inserted and removed.

A second, more-successful method for forming a smooth ice layer starts with the deuterium in the liquid phase and then gradually cools the target through the triple point. The initial thermal environment *inside* the target is shown in Fig. 99.24. The temperature gradient along the interface between the gas and the liquid is determined by the helium gas pressure outside the target and the heat coupled into the deuterium. Properly executed, this process forms a single crystal within the melt that is first observed near the target's equator and then propagates azimuthally and vertically within the shell.

Figure 99.25 shows the same target produced using both methods. It demonstrates the importance of controlling the solidification rate: all parameters other than the temperature difference between the layering sphere and target, which controls the heat flux from the target (and hence the solidification rate), were kept constant; the same target was maintained in the identical position and orientation in the layering sphere, and the same volumetric heating rate was used. The smoother ice layer (2.5-μm rms) was produced at a temperature ~0.1 K

below the triple point; the second, rougher ice layer (4.3-μm rms) was produced at a temperature ~0.2 K below the triple point, in a faster solidification process. This difference in roughness can be attributed only to the intrinsic properties of the ice (the crystallographic structure and how well it attaches to the inner plastic wall). Both images show features that can be eliminated by carrying out the process still closer to the triple point (within 5 to 10 mK).

Ultimately, if the outer surface of the plastic capsule is isothermal, the ice will possess equivalent thickness everywhere if all of the following conditions are identical throughout the capsule: (1) heat conductance through the ice; (2) heat resistance at the ice/plastic interface; (3) heat conductance through the plastic; and (4) volumetric heating into the ice (and plastic). In the above comparison, the importance of the solidification rate on the resulting ice smoothness was demonstrated because only conditions (1) and (2) could vary. The effect of items (3) and (4) remained invariant because the plastic shell and its position in the layering sphere were the same.

One final consideration is to determine how precisely the solidification process must be controlled to achieve a "perfectly" uniform thick layer. The stochastic nature of the freezing process will always cause some variability to the layer quality, and this contribution to the overall roughness will become more important as extraneous, equipment-related perturbations to the ice are eliminated (examples include nonuniform heating or the position of the target in the layering sphere).

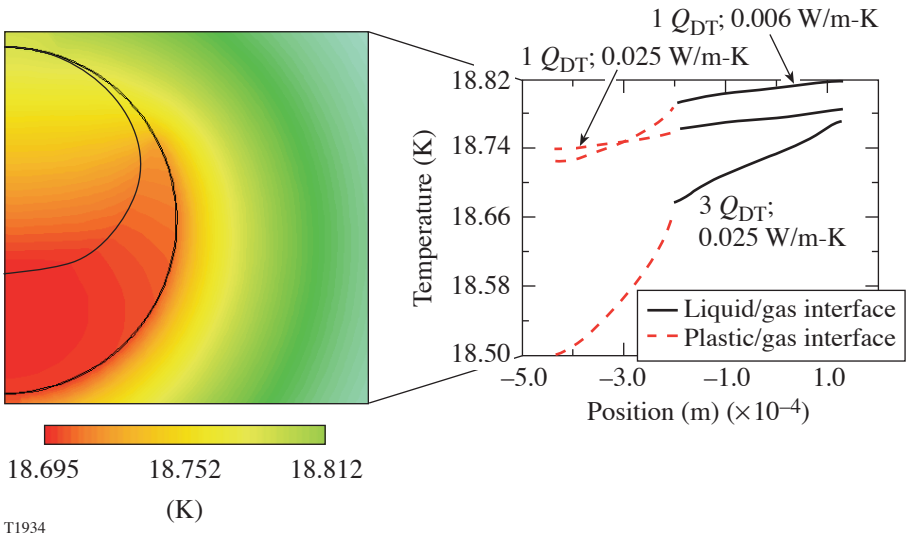

Figure 99.24
Temperature distribution inside a liquid-D_2–containing OMEGA target. Three different volumetric heat loads (1 and 3 Q_{DT}) and two different helium exchange gas pressures, which yield different thermal conductivities, are plotted.

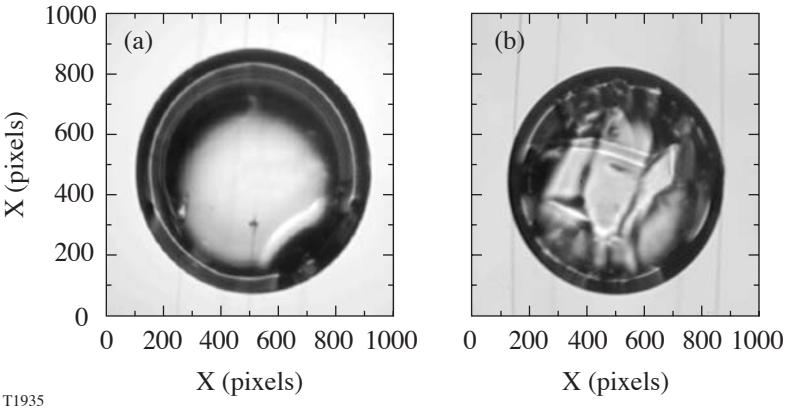

Figure 99.25
Image of the same target with two different ice layers. The first layer (a) is formed gradually at a temperature that is close to the triple-point temperature (within 0.1 K). The second layer (b) occurs when liquid is frozen instantaneously at a temperature and then allowed to layer.

Characterizing the Ice Layer

1. Experimental Configuration

The optical system used to measure the ice-layer roughness is shown in Fig. 99.26. The layering sphere has two pairs of opposing windows oriented along axes corresponding to the viewing axes in the OMEGA target chamber. The windows corresponding to the X- and Y-axis cameras are positioned 26.6° and 12° above and below the equator, respectively, and 110° apart.

The light-emitting diodes that back-illuminate the target are opposite the cameras. The diodes operate at 1 Hz and 0.15 A with a 30-ms to 300-ms exposure. The emission wavelength is 612 nm, i.e., in a spectral region where the deuterium (or tritium) ice does not absorb but where the plastic shell has broadband absorption of 5% to 10%. These exposure conditions permit a target image to be acquired in a sufficiently short period that vibration-induced blurring is minimized. Also, the brief exposure duration minimizes the heat load to the target. Based on measurements, and supported by calculations, the heat load to the target is <10 nW. Operating the diodes at a higher duty cycle and current can produce heat loads (in the plastic shell) that approach 0.1 μW, a value that is a significant fraction of the 10 μW to 30 μW deposited in an OMEGA target by IR radiation during layering. The effect of higher diode-radiation loads on a target is shown in Fig. 99.27. Here, in an extreme example, the diode is seen to deplete the 100-μm ice layer along the illumination axis. That such a drastic effect is induced at high illumination intensities underscores the need for minimizing any nonuniform heat load to the target, including loads from all optical systems associated with positioning the target in the target chamber as well as from the target existence detector.

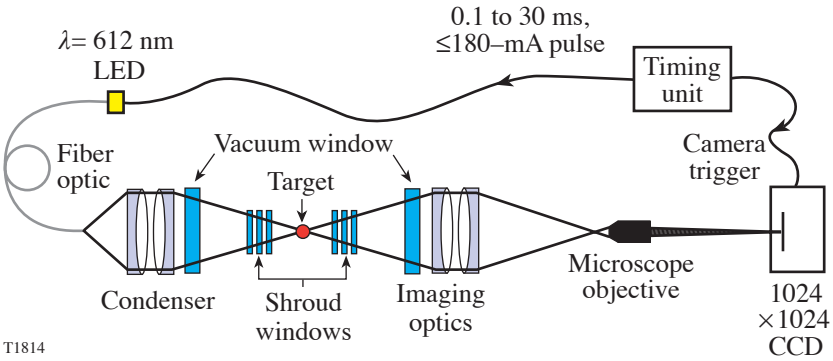

Figure 99.26
Schematic of the optical system used to acquire images of cryogenic targets.

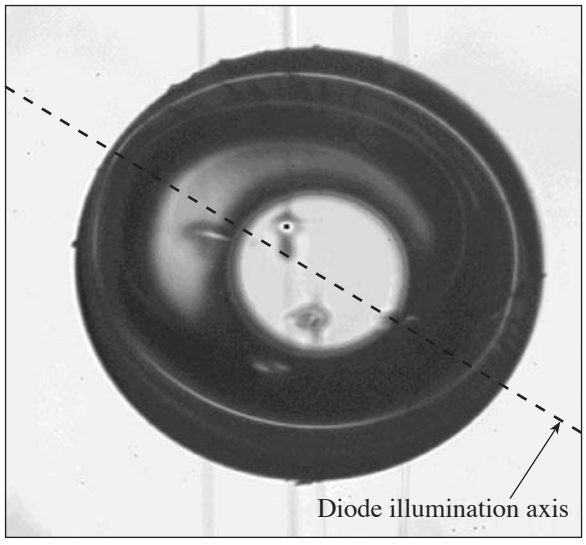

Figure 99.27
The ice layer is distorted (thinner) along the axis of the diode illumination used to backlight the target. The diode light (612 nm) was absorbed in the plastic to create localized hot spots.

2. Numerical Analysis

Backlighting the target provides an image as shown in Fig. 99.28. Notable are the outer limb of the plastic shell and narrow, concentric, circular, bright bands due to light reflecting off the inner ice surface. The brightest band is light reflected from the inner ice surface perpendicular to the illumination axis. Less-intense bands are reflections from different regions of the inner ice surface and may include multiple internal reflections. Only the brightest band is analyzed. The band may vary in intensity, or become discontinuous, due to either scattering centers in the ice (i.e., crystallographic features) or defects on the surface of the plastic shell that deflect light rays that would otherwise be captured by the viewing optics.

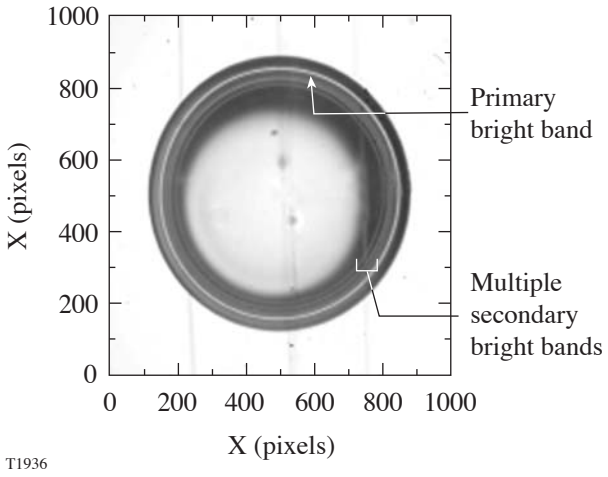

Figure 99.28
An example of a high-quality ice layer where both the primary bright band and multiple secondary bright bands are visible.

This technique, referred to more generally as *shadowgraphy,* yields a 2-D slice through the ice layer. Rotating the target and acquiring an image at each rotational position allows a 3-D tomographic image of the ice layer to be assembled.

The analysis algorithm calculates the center of the target from the outer limb of the plastic capsule and then determines the radial distance from the center to the inner ice surface. The variation in the distance is approximated using a Fourier cosine expansion. The coefficients of the expansion report the spectral power density in each mode. The layer roughness is calculated separately as an rms least-squares fit to the entire data set. The Fourier spectral decomposition better defines how the roughness is distributed. Phase information from the 2-D analysis is not used; that information is more easily visualized from the 3-D analysis.

The camera and optics provide a resolution of ~1.1 μm per pixel, and a total of ~350 pixels comprise the circumference of the bright band. Although the diffraction limit on the resolution is 3 μm to 4 μm, the statistics afforded by the large number of pixels allows the roughness to be determined with a precision better than 0.5 μm. This analysis assumes that the outer ice surface (the one contacting the plastic capsule) is perfectly circular, whereas the actual roughness ranges from 0.2 μm to 0.7 μm (as defined by the roughness and thickness uniformity of the plastic wall); clearly, as the ice roughness approaches the 1-μm goal, the existence of a 0.5- to 0.7-μm roughness due to the plastic will make the ice seem rougher than it really is. An example of this is shown in Fig. 99.29 where the ice roughness was 1.1 μm and the plastic roughness was 0.5 μm.

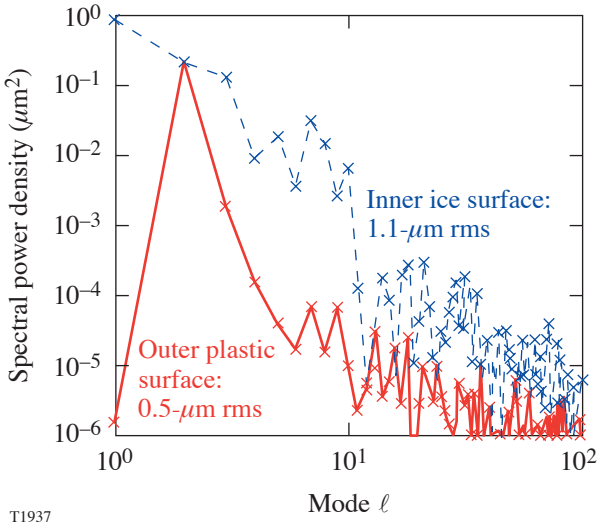

Figure 99.29
The power spectrum of a 100-μm ice layer shows that the smoothness is approaching the goal of 1-μm-rms roughness. The roughness is primarily in spectral modes 1 through 10, with comparatively little power in higher modes.

It is important to know the accuracy and repeatability of the analysis algorithm. Two methods were used to acquire this information: In the first method, a 1-mm sapphire ball with a measured ~0.05-μm-rms roughness (characterized using atomic force microscopy) was inserted into the layering sphere and the outer limb was analyzed with the optical system and software tools. The measured optical roughness was ~0.2 μm (rms), four times the roughness obtained using the more-accurate AFM technique. This suggests that the technique has an amplitude threshold below which the precision is increasingly dominated

by pixelated noise. In the second method, seven successive images of a target were acquired. Multiple ice layers were studied, and the difference between the average value of each data set of seven images and the actual value is shown in Fig. 99.30. A total of 382 data sets were analyzed and showed a repeatability of ±0.1 to 0.2 μm for most ice layers. Targets that vibrated significantly exhibited a greater variability in the roughness (up to 0.7-μm difference), despite the strobing effect of the pulsed illuminator. It is likely that different target views were imaged because a vibrating target also rotates slightly. These data suggest that a minimum of three and maximum of five images of each 2-D great circle be acquired in order to attain statistical confidence in the data.

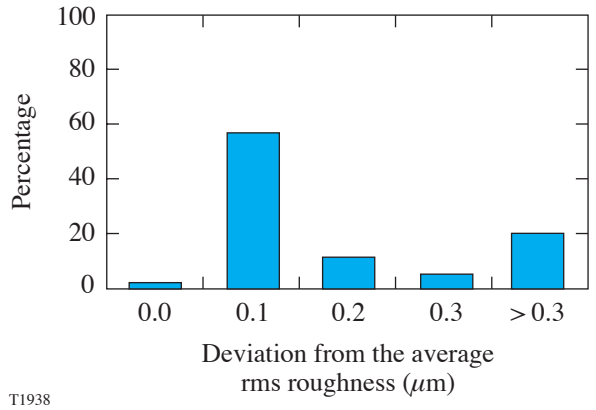

Figure 99.30
Histogram showing the variation of the inner ice surfaces' rms roughness from an average, as determined by the shadowgram analysis routine. The average rms roughness was calculated from seven repeat images of the same ice layer.

Ice-Layer Quality

1. Solidification Process

At the start, deuterium is a liquid with its meniscus extending 3/4 of the way up the side of the capsule. Although it cannot be imaged, a thin, contiguous fluid layer should exist around the entire capsule since liquid hydrogen effectively wets plastics; the contact angle is zero.[4] The temperature is initially 0.05 K to 0.1 K above the triple point and is lowered by 0.2 K to begin solidification. A seed crystal appears first near the equator and expands vertically up the sides of the capsule. This behavior differs from that observed in targets containing fill tubes where a seed crystal is always present at the fill tube (at the top of the target) and the crystal grows from gas condensation.[5] Throughout the process, the target is thermally loaded by 3.16-μm radiation at a constant rate.

To fully solidify the target, the latent heat of fusion must be removed. In an OMEGA-scale target, this amounts to a total of ~2 mJ. The solidification time depends on the temperature difference between the target and the layering sphere and the helium gas that may be in one of two possible pressure regimes. Equation (1) applies to sufficiently high helium-gas pressure (*continuum* or *kinetic* regime), where heat flow is independent of pressure:[6]

$$Q = 2k\left(T_{\text{target}} - T_{\text{layering sphere}}\right) d_i d_o / \left(d_o - d_i\right), \qquad (1)$$

where Q is the heat flow from the target to the layering sphere, d_i is the diameter of the inner sphere, d_o is the diameter of the layering sphere, and k is the thermal conductivity of helium gas. In this application, the only variable parameter in Eq. (1) is the temperature of the layering sphere: the target will completely freeze in <1 s for a temperature gradient of 1 K between the target and the layering-sphere boundary. Since the goal is to slowly freeze the target to achieve a *single* seed crystal from which a single ice crystal can grow, the solidification rate depends strongly on (1) knowing precisely the layering-sphere temperature that *corresponds to the triple point in the target* and (2) maintaining the layering-sphere temperature marginally (10 mK) below this "triple-point-equivalent" value. Rapidly freezing the target forms a polycrystalline ice structure that makes it difficult to observe the bright band and to achieve a smooth ice layer [Fig. 99.25(b)].

This temperature differential can be ascertained by performing the inverse of freezing, i.e., *melting* the ice. Typical volumetric heat loads to the target range from 8 μW to 30 μW. (This value is determined by forming an ice layer using IR light, isolating the IR source, raising the temperature of the layering sphere and target to 18.72 K, and switching on the IR heat source again. The time required for the solid to melt provides an estimate of the heat load since the heat of fusion for deuterium and the mass in the target are accurately known.) These heat loads predict a steady-state temperature difference between the target and the layering sphere of the order of 0.05 K to 0.2 K; the actual temperature difference is 0.7 K to 2 K. Such a discrepancy points toward a helium-gas pressure in the layering sphere well below the continuum limit where thermal conduction depends on gas pressure. This situation is plausible since the gas path to the layering sphere is not leak-tight (an unavoidable "real-world" consequence of the equipment having to provide targets for implosion experiments, as opposed to a single-purpose, scientific test bed).

Equation (1) applies when the mean free path of the gas is significantly shorter (1/100th or less) than the distance between the target and the layering sphere. When the mean free path is of the same order, or larger, than the scale length (the Knudsen number >1), the gas is in the *transition or molecular regime*, and heat transport between the target and the layering sphere is described as[7,8]

$$Q = (a_o/4)\left[(\gamma+1)/(\gamma-1)\right]\sqrt{2R/\pi M} \times P\left(T_{\text{target}} - T_{\text{layering sphere}}\right)\Big/\sqrt{T_{\text{target}}}, \quad (2)$$

where R is the universal gas constant, P is the pressure, M is the molecular weight, γ is the ratio of the specific heat capacity at constant pressure and volume $\left(\gamma = C_p/C_v\right)$, and

$$a_o = \frac{a_1 a_2}{a_2 + \left(\frac{A_2}{A_1}\right)(1-a_2)a_1}, \quad (3)$$

where a_1 (or a_2) is the accommodation coefficient of helium at a surface, A is the surface area, and 1 and 2 refer to the layering sphere and target, respectively.

Operating the layering process at a helium pressure below the continuum limit requires a lower temperature on the layering sphere to freeze the deuterium. This is to compensate for the diminished thermal transport through the gas. Figure 99.31(b) shows this effect.

A second effect of the low helium-gas pressure pertains to the temperature gradient that it establishes around the outside (θ,ϕ) of the plastic shell, which increases the temperature gradient across the void space within the target (Fig. 99.24): the temperature gradient increases from 0.05 K to 0.11 K, for a heat load of 1 Q_{DT}, when the helium pressure is decreased from the continuum to the molecular regime. This temperature gradient is important since it affects the heat flux from the target and the dynamics of crystal growth. Typically, the OMEGA CTHS operates in the transitional region between the kinetic and molecular regimes.

While the target freezes, the ice temperature remains at, or very close to, the triple point temperature of 18.72 K. Once the latent heat of fusion is removed, the target continues to cool until it reaches a temperature where the IR heat load into the target is balanced by the heat flow out of the target. This temperature depends only on the temperature of the layering sphere, the helium-gas pressure, and the heat in the target. There are consequences for lowering this temperature in terms of strain experienced by the ice. The farther the final target temperature reaches below the triple point, the greater the ice strain (ice contracts by ~0.45%/K; contraction in the plastic is negligible over this range). The induced strain adds to any intrinsic strain due to the crystal contorting to the confines of the shell. Once the local strain exceeds the yield point (~0.2% strain),[9] the induced stress will cause the ice to fracture. The radial-thermal-conduction uniformity, and hence the ice-thickness uniformity, will be affected by where, and how extensively, the ice fractures.

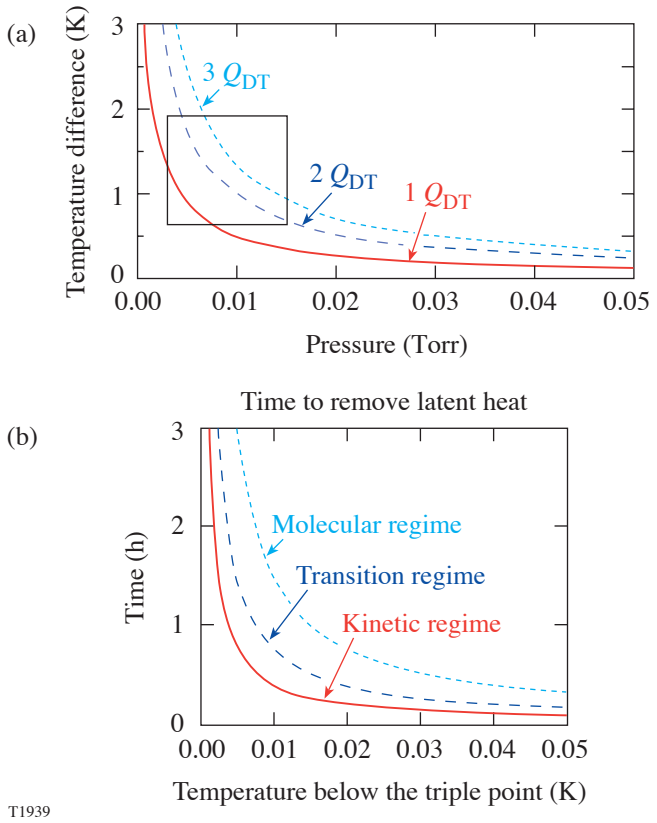

Figure 99.31
(a) The relationship between the helium-gas pressure and the temperature difference between the target and the layering sphere is shown for three heat loads (1, 2, and 3 Q_{DT}) (accommodation coefficient is 0.5). (b) The relationship between the time required to remove the latent heat from the target and the helium pressure and temperature gradient (between the target and the layering sphere). The inset box in (a) shows the typical region of operation.

2. Effect of the Solidification and Layering Process on the Resulting Ice Roughness

The solidification process is inherently stochastic. It depends on where a seed crystal forms, how many seeds form, and how quickly the resulting crystals grow and then interact. The resulting ice morphology, including facets or dislocations in the crystal structure, may influence the thermal-conduction path that in turn affects the final ice roughness.

To separate the effects of ice morphology and external perturbations on the ice roughness, and to quantify the inherent variability in the solidification process, a single target was repeatedly layered and melted using the identical protocol and configuration (the same IR heating power, helium-gas pressure, and target position). For each repetition, the liquid-containing target started at the same initial temperature, and layering was initiated using the same temperature decrement. The roughness of 11 separately formed ice layers is shown in a polar plot in Fig. 99.32. Each layer was rotated through 360°, and a 2-D image was acquired every 15°. The rms roughness of each great circle was plotted against the corresponding rotational angle. Three trends are noticeable: (1) The roughness of each great circle for a particular rotation shows good repeatability. The rms values are within ±1 μm of the average. (2) There is strong correlation between the roughness and the target's rotational orientation (±1-μm variability), and (3) there is significant variability in the roughness of each layer (±2 μm). This test was repeated using two different targets to determine if the rotational correlation was capsule dependent. The targets were layered, melted, and relayered three times with similar results (Fig. 99.33). Each layer's roughness repeated to within ±0.6 μm, and a similar azimuthal dependency of the roughness was observed. These data sug-

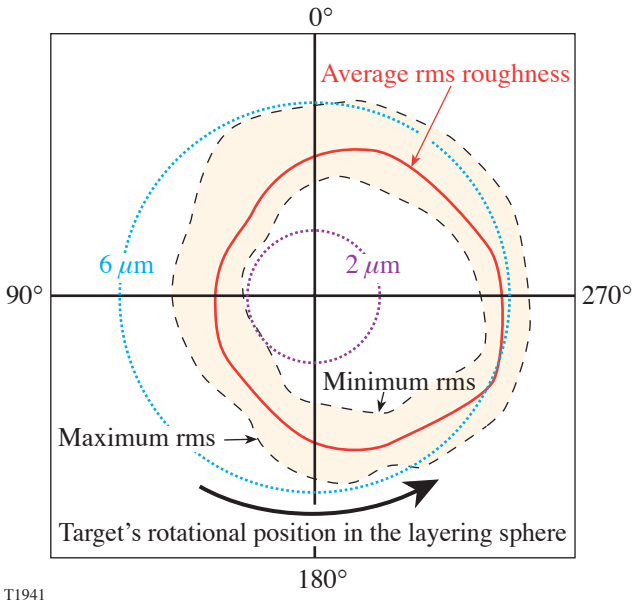

Figure 99.32
Polar plot showing the rms ice roughness of individual 2-D great circles through the target relative to the layering sphere. The average, minimum, and maximum roughness values of 11 different layers are shown for each 15° rotational angle.

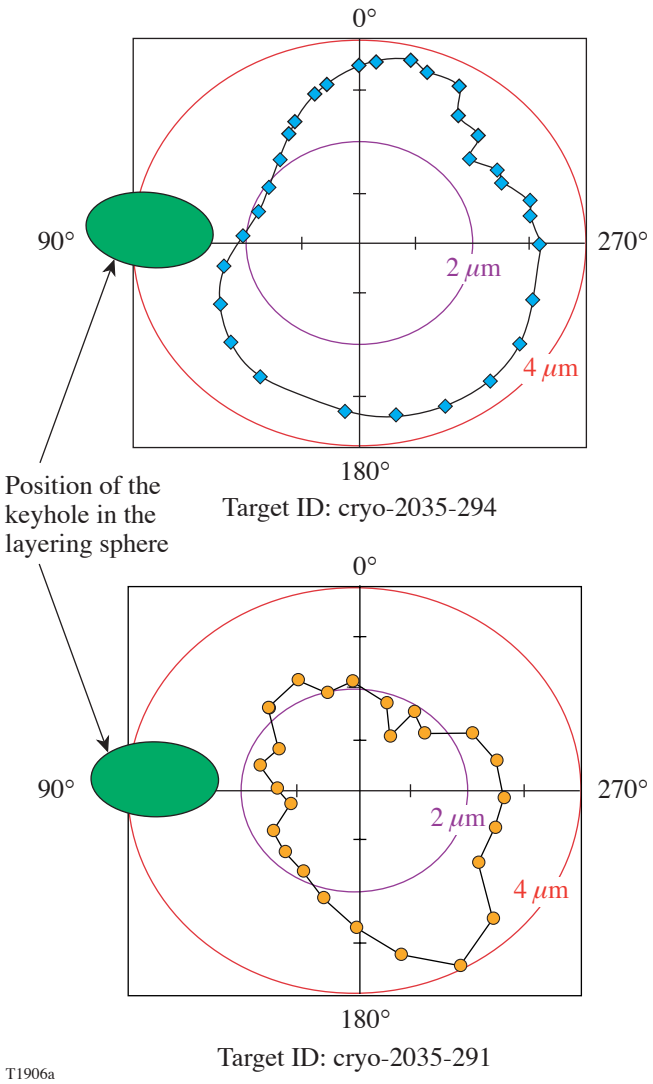

Figure 99.33
Polar plots showing the rms roughness of 2-D great circles relative to the layering sphere. Three separate ice layers were averaged for each plot. Each plot corresponds to a separate target.

gest the following: (1) the geometry of the layering sphere, not the plastic shell, is responsible for the azimuthal variation in roughness; and (2) the solidification and ice-layering process alone produced a variability of ±0.6- to 1-μm variability in the ice roughness.

Three-dimensional images of the ice-layer thickness of four of these layers (same target and layering conditions) are shown in Fig. 99.34. All layers have comparable roughness. The roughness distribution is similar: isolated regions of thicker ice are located at each target's equator and at varying azimuthal angles.

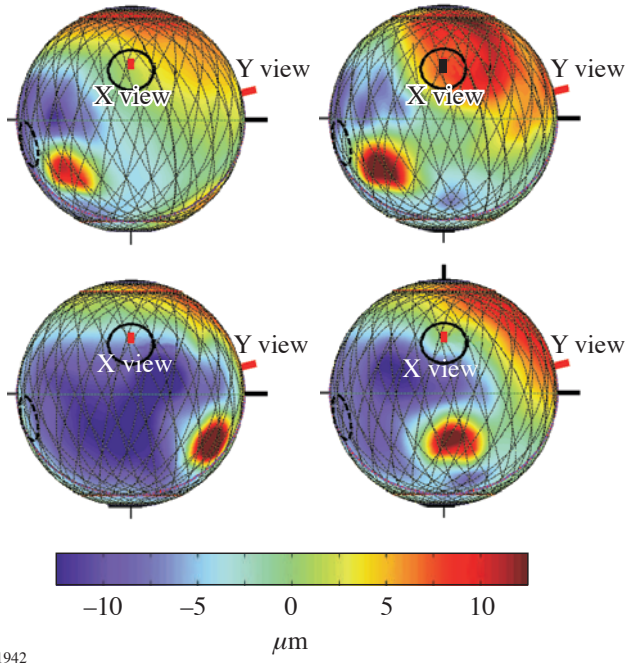

Figure 99.34
Three-dimensional plots of the ice thickness. Four separately formed ice layers in the same target are shown.

3. Effect of External Perturbations on the Ice-Layer Roughness

The environment surrounding the target will affect the ice-layer quality if there is insufficient control of the heat flows into and out of the target or if nonuniform illumination or thermal conditions exist. The stability of the heat flow *into* the target depends on the stability of the IR light source. The stability of the heat flow *out of* the target depends on a constant helium-gas pressure and constant temperature on the layering sphere. Uniform illumination of the target requires the layering sphere to perform as an integrating sphere to ensure uniform volumetric heating (no hot spots). Also, a uniform thermal boundary condition requires the layering sphere to be isothermal so that the outer surface of the plastic shell is isothermal *when* the ice is uniformly thick. The consequences of variations in any of these parameters are addressed next.

a. Stability of the IR source. The IR source is a pulsed optical parametric oscillator (OPO) supplied by Aculight, Inc. The pulse repetition rate is 30 kHz; the wavelength is tunable over the 2.9- to 3.3-μm range with a bandwidth of 10 nm. The IR light transits through a 60-ft optical fiber into the layering sphere. The layering sphere contains an indium antinomide (InSb) detector that measures the IR intensity and provides feedback for maintaining constant power. The maximum OPO output power is 200 mW, which is attenuated 60% to 80% by the fiber and coupling connectors. Of the 40 mW to 80 mW injected into the layering/integrating sphere, a maximum of 30 μW is coupled into the target. Reasons for this low efficiency are the low Q of the integrating sphere (ray tracing suggests that a ray traverses the sphere fewer than 20 times before exiting) and the low absorption in the 100-μm ice layer (~4%).

The long-term stability of the OPO power is important since the target's temperature needs to be below, but as close as possible to, the triple point. This limits the crystal to growing from a single seed, slows the growth rate, and minimizes the volume contraction that occurs when solidification is completed. Any drift in the OPO output power over the layering period may melt the ice crystal. For example, consider a layered target that is 0.01 K below the triple point: a +1% drift (increase) in OPO power (corresponding to an 0.08-μW variation) equates to a 0.001-K change in the target's temperature if the helium pressure is in the continuum regime; however, if the pressure is below the continuum limit, the temperature may increase by up to 0.060 K, which would melt the ice. A negative drift in OPO power does not lower the target's temperature, which is clamped at the triple point until solidification is complete, but will cause an imbalance in the overall heat flow and hence the solidification rate. The parametric relationship between the change in the target's temperature and the heat load and helium pressure for a 1% increase in the OPO power is shown in Fig. 99.35. As the layering-sphere temperature is controlled to ±0.001 K, it is the stability of the OPO source that controls the stability of the target's temperature.

Typical data for the long-term power stability of the OPO are shown in Fig. 99.36. The OPO drifts by ±4% over a 24-h period. When operated under closed-loop control, the drift in

power diminishes to less than ±1%. Short-term power fluctuations involving energy change substantially less than the latent heat of fusion may not melt or flash freeze the deuterium. They may, however, affect the crystal formation, i.e., a 1-μW increase in power (equal to 4% of 3 Q_{DT}), which places the target temperature above the triple point, will cause the target to slump within 10 min and to melt within a half hour.

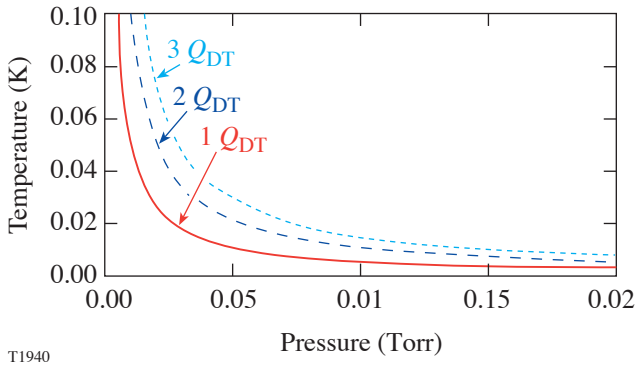

Figure 99.35
Graph showing the change in the target's temperature when the OPO power increases by 1%. The dependency of this response on different heat loads (1, 2, and 3 Q_{DT}) and helium-gas pressures is shown. The accommodation coefficient is 0.5.

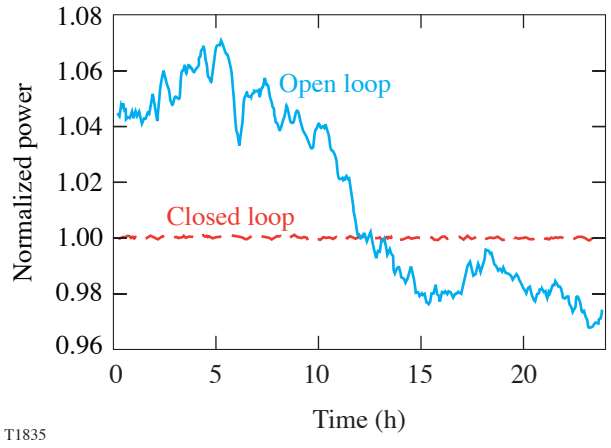

Figure 99.36
Plot showing the stability of the OPO when it is operated in closed-loop control and the magnitude of the drift when operated without feedback control.

b. Illumination uniformity of the layering sphere. As described earlier, the layering sphere containing the target is also the integrating sphere. The integrating feature is brought about by a purposely roughened, highly reflective Lambertian surface (gold coated) that is to provide a uniform IR intensity throughout the sphere. There are features, however, in the layering sphere that affect this illumination uniformity, including the four sapphire windows (~6-mm diam) and an entry hole at the base of the sphere used to insert and remove the target. The area of the entry hole is 2% to 3% of the total area and is the largest single feature affecting illumination uniformity. The effect of the shadow cast by this feature on the target was assessed by (1) tracing rays through the target to determine spatially where the heat was deposited in the ice, and (2) calculating how the resultant heat deposition affected the ice-layer thickness.

The ray-tracing calculation modeled only those rays that would originate from the "hole" region; rays originating elsewhere are uniformly distributed throughout the ice. The path of the rays through the ice was calculated from the refractive indices of the plastic, the ice, and the internal gas void, and the Fresnel coefficients when the angle of the ray relative to a surface was below a threshold.[10] The model was axisymmetric, and regions of the ice were zoned according to the ray density. Importantly, the ray density was not distributed isotropically (see Fig. 99.37). Because of the focusing effect of the ice, the density of rays at the target's rear surface is marginally greater than at the front surface. The largest variation in ray density was along a great circle perpendicular to the incident rays, but this was over a small area.

The assumed volumetric heat load into an axisymmetric thermal model of a cryogenic target was 8 μW (equivalent to the tritium decay energy in a DT target). Of this value, an average of 0.18 μW was subtracted from the target because of the absent rays that would have otherwise originated from the hole region. (This value is proportional to the ratio of the area of the hole to that of the entire surface.) The exact assignment of power into each zone was normalized to the ray density, where regions with the *highest* density of rays received the *largest reduction* in heat.

The resulting temperature profile on the internal ice surface was calculated using the computational fluid dynamic code FLUENT.[11] Simulating the ice-layering process manually, the ice-layer position was adjusted and the temperature distribution recalculated until the inner ice surface was isothermal.

The resulting ice-layer thickness is shown in Fig. 99.38. Spectral analysis of this great circle yields an ice roughness of ~4-μm rms.

Experimental evidence of this possible perturbation source is not straightforward since many competing sources can affect the ice-layer thickness. By examining only the smoothest targets, the contribution of other sources of roughness to the ice is reduced, which may allow the effect of the layering sphere to be more noticeable. Figures 99.39(a)–99.39(c) show a target with an average ice rms roughness of 1.2 μm (determined by averaging the roughness of 24 2-D great circles around a target) that possesses thinner ice facing the keyhole (bottom of the target) than at the rear surface (top of the target), which are the general locations predicted by the ray-tracing analysis. The light region in the image [Figs. 99.39(a)–99.39(c)] indicates a region of thicker ice and corresponds to the area where fewer rays coincide, possibly because of the shadow cast by the hole in the layering sphere.

The calculated ice thickness from the thermal model is shown in Fig. 99.39(d) for a 2-D great circle oriented along the same axis as the hole in the layering sphere. The volumetric heat load was obtained from the ray-trace calculation. The ice is thinnest where the target faces the hole (the darker hemisphere), and thicker opposite the hole. This pattern is similar to what is seen experimentally with the main difference being that the thick region of ice should be cylindrically symmetrical around the target's equator. While this is not conclusive evidence that the hole in the layering sphere is responsible for the observed ice-thickness variation, this possibility warrants a more-detailed study. Two limitations of the thermal model are that (1) it is only an axisymmetric model, not a 3-D model so that the modeled hole was circular, not of the more-complex

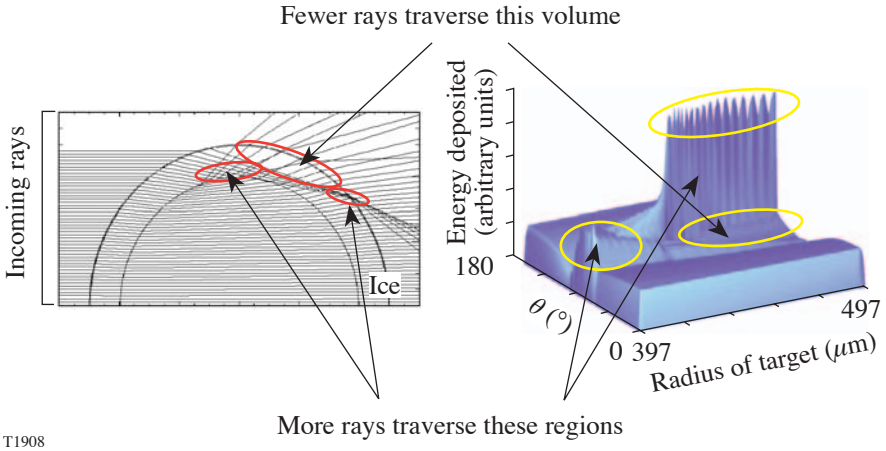

Figure 99.37
Ray trace through a symmetrical target showing where the IR energy is deposited in the ice. The focusing effect of the ice and internal reflection from the inner ice surface are responsible for the behavior. Q is the volumetric heat load.

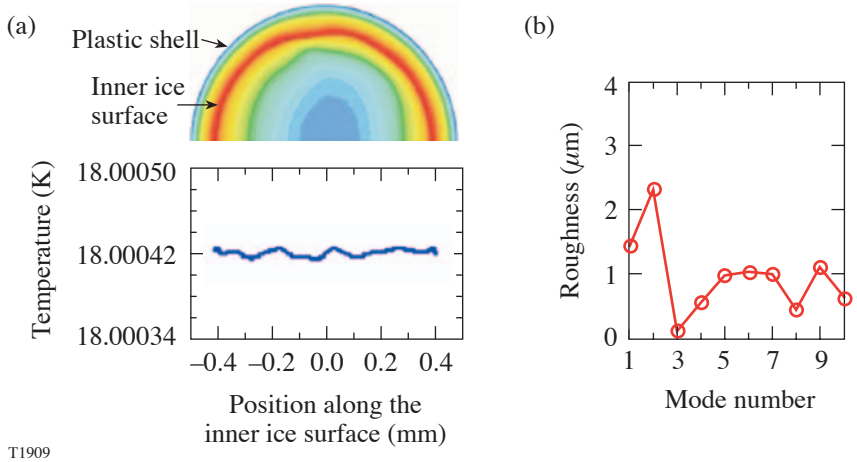

Figure 99.38
(a) Isotherms within an ice layer once the ice thickness is adjusted to account for the lack of illumination on the target (caused by the keyhole in the layering sphere). The associated power spectrum is shown in (b).

trapezoidal geometry of the actual hole, and (2) a constant-temperature thermal boundary condition was imposed on the outer surface of the target to provide sufficient grid (spatial) resolution for the calculation. This would exaggerate the ice thickness at the equator. The boundary condition should be on the layering sphere wall.

Lastly, the calculated 4-μm-rms roughness is greater than the roughness observed in any of the individual 2-D analyses of a target: this stems from the calculated 2-D great circle going through both the north and south poles—an orientation that cannot be viewed by either the X or Y viewing axes. Instead, the viewable 2-D great circles intersect only a portion of the great circle calculated above. The orientation of the ice-thickness distribution becomes apparent only after the 3-D surface is generated.

c. Stability of the target temperature and helium exchange gas. The temperature of the layering sphere is controlled to ±1 mK, using Cernox™ temperature sensors and heaters with a highly damped feedback-control algorithm. Fluctuations in target temperature are expected to be less than 1 mK, owing to the additional buffer provided by the low thermal diffusivity of the helium exchange gas. The effect of this temperature instability is insignificant compared to the effect of the power drift in the OPO, so much so that the temperature stability of the layering sphere does not affect the layering process.

It is important that the helium-gas pressure be stable for the duration of the layering. A variable heat flux would risk rapid freezing, the formation of multiple crystal growth sites, and the subsequent propagation of multiple crystals and facets. There is no experimental evidence that the gas pressure may vary.

An issue larger than the pressure stability is the lack of knowledge of the absolute pressure. This complicates, but does not compromise, the process by prolonging the time it takes to determine an optimal temperature setting on the layering sphere to commence layering. It may also be beneficial to be able to adjust the pressure in controlling temperature gradients around the target.

Furthermore, the accuracy of the target-temperature measurement depends also on the time available to make that determination. Experiments that freeze and melt the target at very slow rates (5 mK per two hours) ensure complete equilibration between the target's temperature and the temperature of the layering sphere, which compensates for the small heat-flow changes that occur relative to the latent heat of fusion. Under these conditions, it is possible to determine the target temperature to within 5 mK of its absolute value. Under such tight control, a geometrical effect comes into play: the liquid freezes at a slightly different temperature than the one at which the ice melts (because the slumped liquid layer covers only a portion of the plastic shell through which heat is removed).

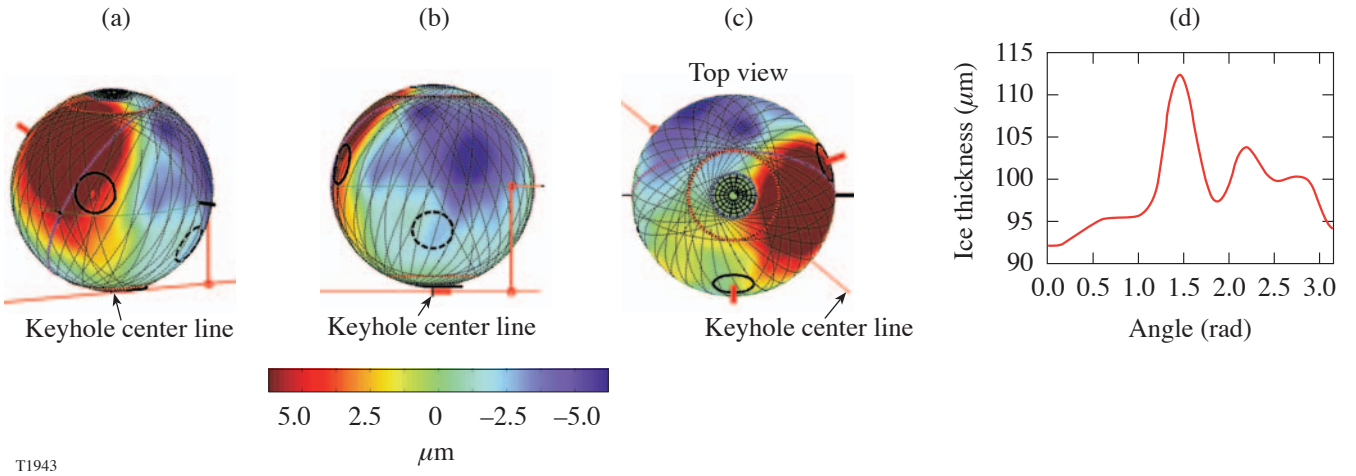

Figure 99.39
Images (a), (b), and (c) show the ice-thickness distribution in a target where the average ice rms roughness is 1.2 μm. The thickness variation along a great circle through the keyhole line is ~8 μm peak-to-valley. The calculated thickness variation, from the ray trace and thermal model, from the bottom of the target to the top and along the axis of the hole is shown in (d).

Thermal Analysis

The thermal environment within and around the target was modeled to quantify the thermal gradients that exist during the layering process. The results offered a better understanding of the layering process's sensitivity to extrinsically controllable and coupled parameters: IR power, gas pressure, and the temperature on the layering sphere. The primary motivation for this model was derived from an uncertainty about how accurately the solidification process can be controlled and what level of control was required for the desired ice-layer quality. Looking forward, such an analysis also helps to better determine the thermal requirements to refine cryogenic equipment.

4. Initial Phase of Forming the Ice Layer

The modeling results of the thermal environment at the initial stage of forming a layer are shown in Fig. 99.24: A melted target is centered in the layering sphere at a temperature slightly above the triple point. The temperature along the inner liquid surface varies between 0.05 K and 0.1 K, depending on the helium pressure. Based on actual experimental values, the model uses the following input parameters: The temperature on the layering sphere is 18.52 K, in accordance with the diminished helium-gas conductivity (0.006 W/m-K) due to the gas pressure being below the continuum limit. The heat load into the liquid and plastic is 1 Q_{DT} (the amount of heat from an equimolar DT solution). Raising the heat coupled into the target to 3 Q_{DT} raises the temperature gradient to 0.25 K.

With a 0.1-K temperature gradient around the target's external wall, and the average temperature of the target being within 0.005 K of the triple point, the liquid at the top of the target should form a crystal. If it does, the crystal should grow from this position. In practice, such a crystal growing from the top and propagating downward is not observed. Rather, the liquid around the equator of the target freezes first and a crystal grows upward (and in thickness) by vapor condensing on the crystal. Simultaneously, the crystal grows downward into the liquid melt, following classical solidification processes.

Multiple seed crystals form when the temperature decrement used to initiate freezing is large, and a low-quality, multifaceted, polycrystalline layer results. The parametric correlation between temperature difference, pressure, and heat flow from the target is shown in Fig. 99.31. The desirable operating pressure regime is in the flat portion of the curve, from 0.02 to 0.05 Torr, where the temperature gradient between the target and the wall of the layering sphere changes very little with temperature.

Even if slow solidification parameters, which favor single-crystal nucleation, and slow propagation are used, a layer will form within 1 h (Fig. 99.40). The rms roughness after that time is better than 10 μm.

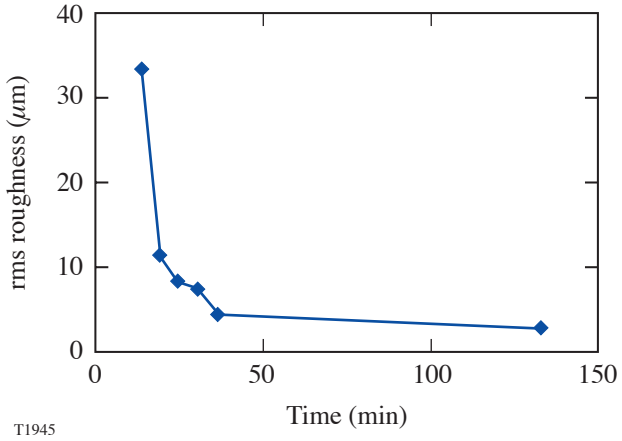

Figure 99.40
The time dependency of the ice-layer formation process indicates that an acceptably smooth ice layer can be achieved in under 3 h.

5. Final Phase of Forming the Ice Layer

Once the ice is mostly symmetrically distributed around the shell, only a small mass needs to be redistributed to create a uniform thickness. The time for this process depends on the sublimation rate, the temperature gradient along the ice/gas interface, and the diffusivity of the deuterium gas.

The sublimation rate depends on the difference between the gas pressure over the solid and the saturated vapor pressure. The pressure/temperature relationship for normal deuterium (near the triple point) is given by the equation[12]

$$P^{\text{vapor}} = \exp\left[19.192 - 177.48/T + 0.00663(T - 16.5\ \text{K})^2\right], \quad (4)$$

where T is the temperature and the rate of sublimation is[13]

$$dm/dt = \left(P^{\text{vapor}} - P^{\text{saturated}}\right) S/\sqrt{2\pi MRT}, \quad (5)$$

where m is mass, P is the pressure, M is the molecular mass, R is the universal gas constant, T is the temperature, and S is the sticking coefficient, which is ~1 for vapor in equilibrium with its solid.

As the ice layer converges to a constant thickness, the temperature gradient along its internal surface decreases. This decreases the vapor pressure and density gradients across the gas void, slowing the layering process. For an ice layer with a peak-to-valley thickness variation of less than 5 μm, the temperature variation along the inner ice surface is less than 0.001 K. This corresponds to a gas-density variation of less than 0.001%. The density/temperature relationship is shown in Fig. 99.41.

Figure 99.40 shows the measured change in the layer roughness of one shell as it converges over time to a 1.8-μm final roughness. The heat load into this target was ~2 Q_{DT}. The process took <3 h; during the last ~100 min, the layer smoothed from 5 μm to 2 μm, corresponding to ~10^{-6} of the total mass being redistributed. The associated temperature variation around the inner surface of the ice decreased from 1.4 mK to 0.15 mK (see Fig. 99.42; the range accounts for the uncertain helium-gas pressure, the converging thickness, and how well centered

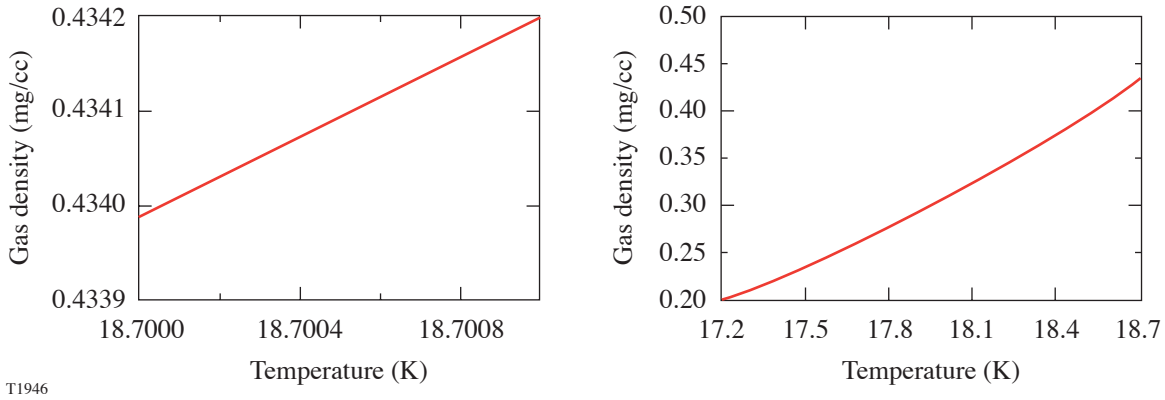

Figure 99.41
The relationship between the gas density and the temperature of the deuterium vapor.

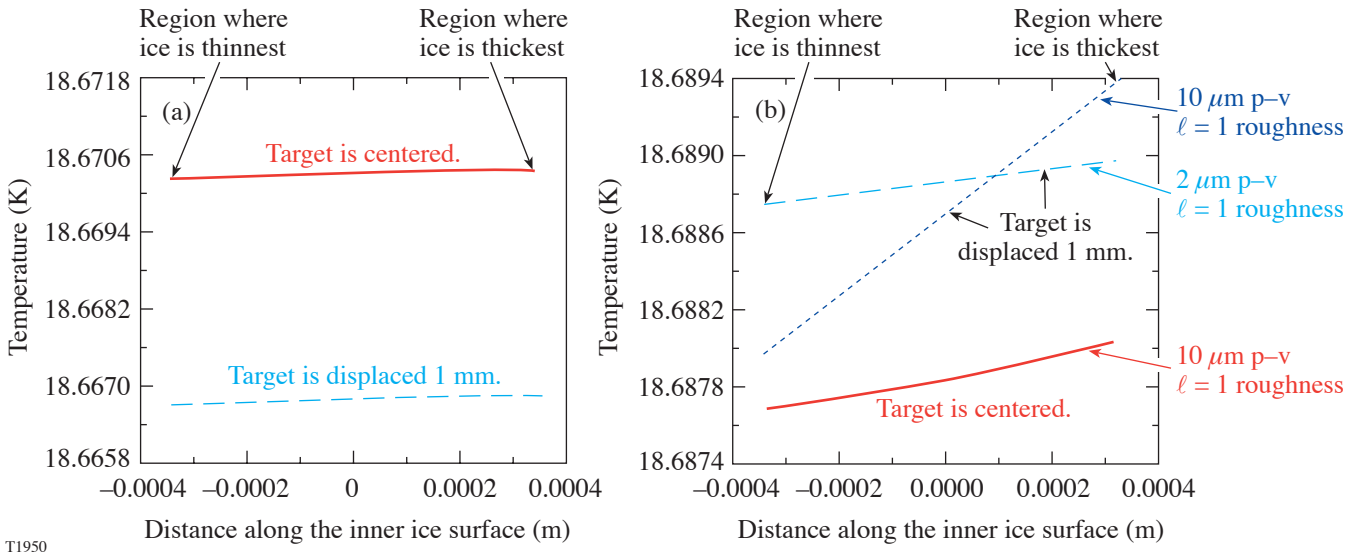

Figure 99.42
The temperature gradient on the inner ice surface is shown for varying conditions: (a) The ice layer has a 2-μm peak-to-valley (p–v) thickness variation, 1-Q_{DT} volumetric heat load, and sufficient helium exchange gas for the system to be in the kinetic gas region. The effect of decentering the target by 1 mm in the layering sphere on the temperature gradient is negligible. (b) This shows the effect of higher roughness, higher heat loads (2 Q_{DT}), and lower gas pressures (thermal conductivity is 1/5 the continuum regime value) on the temperature gradient on the inner ice surface.

the target was in the layering sphere), and the gas density gradient decreased from 0.09% to 0.003%. This density gradient should produce a substantially faster layering time than is observed if gas phase diffusion was the rate-limiting step (the diffusion coefficient is 1.4×10^{-6} m^2/s). Similarly, the D_2 pressure gradients should produce a faster layering rate than observed if the sublimation rate was the rate-limiting step. This infers that the density/pressure gradient is much lower than predicted for the measured ice thickness because the target is closer to an isothermal inner surface than the model predicts. This is achievable only if there is a variable thermal resistance around the target.

Historically, there has been an implicit assumption that the radial thermal resistance of the target is uniform for all (θ, ϕ) polar angles, and if it was nonuniform, the scale length would be sufficiently small for the consequences to be negligible. However, since the ice smoothness infrequently achieves the goal of 1-μm rms but more often is 2 to 3 μm, the validity of that assumption needs to be questioned. There are two parts to this evaluation: (1) the radial thermal resistance of the ice itself, and (2) the thermal resistance across the ice/plastic interface, which is not necessarily equal for all angles θ and ϕ. Two other possibilities are addressed later: (a) the plastic-wall thickness may not be constant and hence contribute a variable-distance thermal path, and (b) the outer plastic surface may not be isothermal.

Given the geometry and size of the target, it is not possible to *measure* the thermal-resistance uniformity between the ice and the plastic, or within the ice itself. Its presence can only be inferred by eliminating other perturbations to the ice. Thermal conduction (k) is proportional to

$$k \sim C_s \rho_s U \lambda, \tag{6}$$

where C_s is the crystal-lattice heat capacity, ρ_s is the density, U is the speed of sound, and λ is the phonon mean-free path. Of these, the phonon mean-free path is the most likely to vary and is affected by (a) the temperature, which influences the phonon density and causes phonon–phonon scattering, (b) the crystal size since grain boundaries scatter phonons, and (c) the local density of deuterium in the molecular $J = 1$ rotational state (J is the spin quantum number). At constant temperature, any variability would be caused by a disproportional distribution of either crystallite sizes or deuterium in the $J = 1$ rotational state (one-third of deuterium is in the $J = 1$ rotational state; the remainder is in the $J = 0$ state), which may occur if deuterium fractionates during the layering process (deuterium's triple point is 0.4 K lower if all the molecules are in the $J = 0$ state). While these are theoretically possible, they seem unlikely.

A second possibility for, and more likely the cause of, a variable thermal resistance is derived from the ice being partially detached from the plastic. If this occurred over a sufficiently wide cord length (of 100 μm or more), the thermal resistance between the inner ice surface and the plastic wall would rise appreciably, even if the gap thickness was very small (thermal conductivity of the gas is 2% that of the ice). The resulting higher ice temperature would cause the ice layer to thin in order to preserve an isothermal inner surface.

Figure 99.43 shows a cryogenic target with a pronounced gap between the ice and the plastic shell. This layer (~20-μm rms roughness) was obtained at a low heat load of ~0.2 Q_{DT}. Raising the heat load to 1 Q_{DT} eliminated the gap, due to the intrinsic layering process, and improved the roughness to 6 to 8 μm. While similar voids were not visible at more-typical 1- to 3-Q_{DT} heat loads, this is not proof that a thin delamination does not exist nor that any thermal resistance at the interface vanishes. It is possible that rapidly freezing a target causes precisely these delaminations, which makes it impossible to form high-quality layers. Figure 99.44 shows a thermal model and resulting ice-roughness power spectrum if a 1-μm-thick void with a length of 200 μm existed at the ice/plastic interface. The resulting rms roughness is 4 μm.

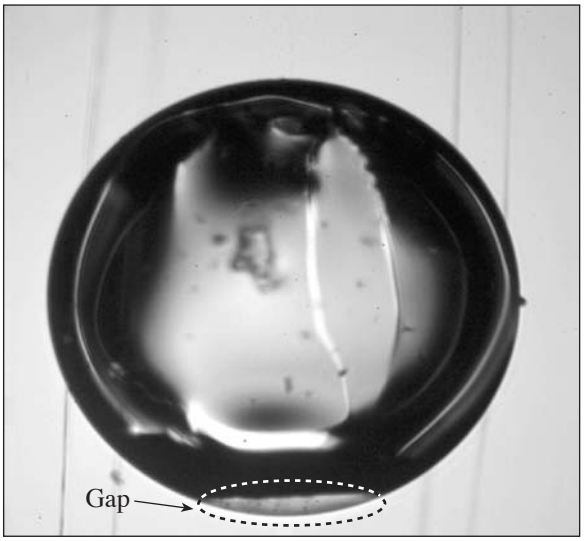

T1859

Figure 99.43
Image of a cryogenic target showing a gap between the plastic and the ice layer.

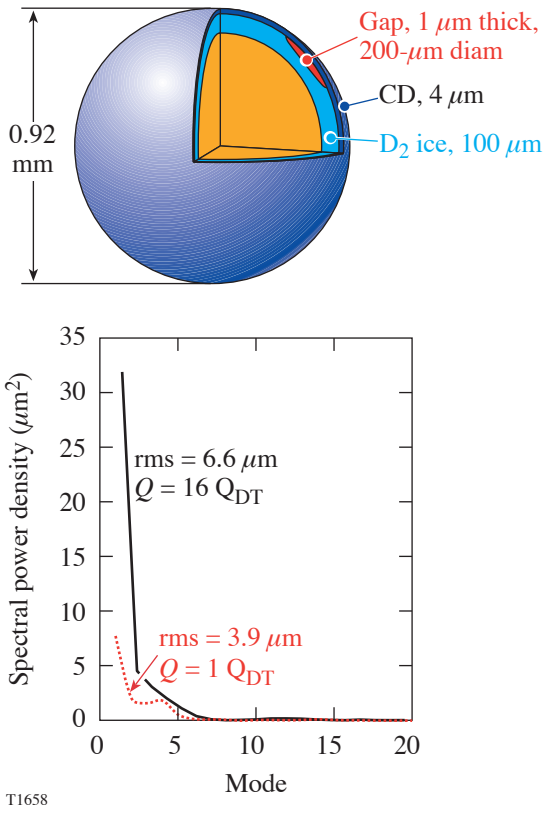

Figure 99.44
Thermal model showing the effect of a 1-μm-thick, 200-μm-diam gap between the ice and plastic on the uniformity of the ice layer.

Another method of affecting the inner ice temperature without changing the ice thickness is for the plastic wall to have variable thickness: if it is thicker on one side of the shell, it will provide a larger local thermal resistance that will make the inner ice surface warmer and will cause the ice layer to thin, relative to the opposing side, to maintain the isothermal property. For example, the thermal conductivity of plastic is one-tenth that of ice, so a 0.1-μm peak-to-valley nonconcentricity in the shell wall (the maximum allowable) would produce an ~1-μm peak-to-valley nonconcentricity in the ice wall. Table 99.I shows the effect of an extreme (0.75-μm) nonconcentricity in the wall of the plastic shell.

Lastly, the position of the target in the layering sphere during the solidification process may affect the eventual uniformity of the ice-layer thickness. It is possible that not centering a target in the layering sphere may result in the inner ice surface becoming isothermal before the ice is uniformly thick. This would occur if the side of the target with thicker ice was closer to the layering sphere. The following calculations investigate the sensitivity of the temperature gradient on the inner ice surface to the target's position in the layering sphere. A target with a 1-μm rough ice layer centered in the layering sphere will possess a temperature variation of 115 μK along the inner ice surface. Displacing the target by 1 mm within the layering sphere changes this variation by a maximum of 15 μK, depending on the alignment of the target's misplacement and ice-thickness variation. If the ice layer was perfectly smooth,

Table 99.I: The temperature gradient along the inner ice surface is calculated for different helium-gas thermal conductivities (due to low gas pressure), positional alignment in the layering sphere, and the effect of a nonconcentric plastic-shell wall.

Peak-to-valley nonconcentricity (ℓ = 1 roughness) in the ice layer	Thermal conductivity of the helium exchange gas (W/m-K)	Position of the target in the layering sphere	
		Centered	Displaced 1 mm from the center[a]
2 μm	0.025	0.115 mK	0.10 to 0.13 mK
		0.190 mK[b]	
	0.006	0.285 mK	0.27 to 0.30 mK
10 μm	0.025		0.55 to 0.60 mK
	0.006		1.42 to 1.44 mK

[a]These values cover the maximum/minimum range that depends on how the ice thickness variation is oriented relative to the target position in the layering sphere.
[b]The plastic-shell wall possessed a 0.75-μm nonconcentricity.

the induced temperature gradient would be only 5 μK for a target displacement of 1 mm. At lower helium pressures (where we currently operate), the temperature gradient around the inner ice surface would be greater (285 μK), but the sensitivity to target position would be the same. Repeating the same calculation for a 10-μm peak-to-valley ice-thickness variation yields a similar proportional trend (see Table 99.I). It is desirable for the temperature variation on the inner ice surface for any ice-thickness variation to be as large as possible to maximize the layering driving force, and for the inner ice surface to be isothermal where the ice is uniformly thick. This will decrease the time it takes for the ice surface to become isothermal. In summary, these data suggest that misplacing the target by 1 mm from the center of the layering sphere will not affect the ability to form an ice layer with 1-μm-rms roughness.

The smoothest target obtained possessed an average ice roughness of 1.2-μm rms; it took 3 h for the liquid to form an ice layer with 1.5-μm-rms average roughness and an additional two days for it to decrease to 1.2 μm. This added time may reflect the gradual mass redistribution that accompanies a very small temperature gradient on the inner ice surface.

Cooling Targets Below the Triple Point

The internal gas density of a cryogenic target is required to be $\sim 0.2 \times 10^{-3}$ g/cm^3, corresponding to a temperature that is ~1.5 K below the triple point (Fig. 99.41). Cooling the target by this much densifies the ice but has no effect on the plastic. Because the ice is attached to the plastic, a strain of ~1% is induced either in the ice or at the interface between the ice and the plastic. This strain is in addition to existing strains that may have developed during solidification. The resulting stress may cause the ice to delaminate from the plastic, or if the adhesion is sufficiently great, the ice may rupture along existing crystallographic planes or defects. Both of these events can affect the ice roughness.

It has been conclusively determined from numerous experiments that the only possible method for meeting both the ice-quality and the sub-triple-point-temperature specification is to form an initial high-quality ice layer and then cool it. For a sufficiently slowly cooled target, the ice quality can be preserved. Figure 99.45(a) shows the results for two different but comparably smooth targets that were cooled at slow rates: 0.02 K and 0.03 K every 20 and 60 min, respectively. The slow rate allowed the strain that was induced during cooling to be relieved before further strain was incurred upon additional cooling. The target that was cooled at the faster rate experienced a marginal increase in roughness [Fig. 99.45(b)], while the second target was unaffected. It is premature to attribute the difference in behavior to the cooling ramps; this is the subject of further experiments. In a separate experiment a target that had roughened during cooling recovered its original smoothness when it was annealed for 18 h [Fig. 99.45(c)]. This behavior, however, does not always occur: the ice shows the same variable behavior that is seen when targets are repeatedly frozen, melted, and refrozen using identical conditions, a behavior that depends on the specifics of the ice crystal.

One expected consequence of decreasing the ice temperature is an increased likelihood for the ice surface to form facets that would generate a sawtooth-like texture and increase the high-frequency roughness. Experimentally, when increased roughness was measured, that roughness was primarily in the lower spectral modes, although the roughness also increased in modes up to 100 (Fig. 99.46). This outcome may be explained by structural changes occurring in the ice as it cools, changes that affect the radial thermal resistance of the ice around the target, which perturbs the isothermal condition on the inner ice surface that causes the ice to relayer. The subsequent ability of the ice to, in some instances, "anneal" these defects and to recover its original smoothness may depend on the type of defect that caused the initial perturbation to the ice.

Effect of Ambient Radiation on the Cryogenic Target

Removing the thermal shrouds exposes the cryogenic target to blackbody radiation from the target chamber, which is calculated from Plank's radiation law to be 0.0047 W. The effect of this heat load on the smoothness of the ice surface and the internal gas density determines the maximum time the target can be exposed before it has to be imploded.

The linear motor used to retract the thermal shrouds can achieve a velocity of 5 ms^{-1} using a constant acceleration of 25 ms^{-2}. This corresponds to the target being exposed to ambient radiation for 0.05 s. The quality of the ice layer moments before implosion is determined using a high-resolution camera inside the target chamber to capture an image of the cryogenic target. The ice layer's smoothness does not appear to be degraded by this exposure time, which is encouraging; however, there is no way to measure the density (or temperature) of the gas in the center of the target. This information can be determined only by calculation. Should calculations also show that the rise in the density of the gas is sufficiently slow, it would be possible to slow the shroud's retraction. The extra time would allow any vibration in the target to be attenuated for longer, thereby allowing the target to be better centered in the target chamber.

Data from the camera inside the target chamber provided time-lapse images [Fig. 99.47(a)] that show how the cryogenic target behaves when the thermal shrouds are removed and the target is not imploded: first, the ice was observed to rotate inside the plastic shell (this occurred during the initial 2 s); then, as the liquid fraction increased, the ice/liquid slurry slumped (within 5 s) and melted after 10 s. The liquid continued to vaporize and the target exploded after 78 s. Immediately before the target exploded, it became transparent, indicating that the temperature had surpassed the critical point, which is the highest temperature where vapor and liquid coexist. Separate experiments determined that the temperature at which an OMEGA cryogenic target explodes is 43±1 K.

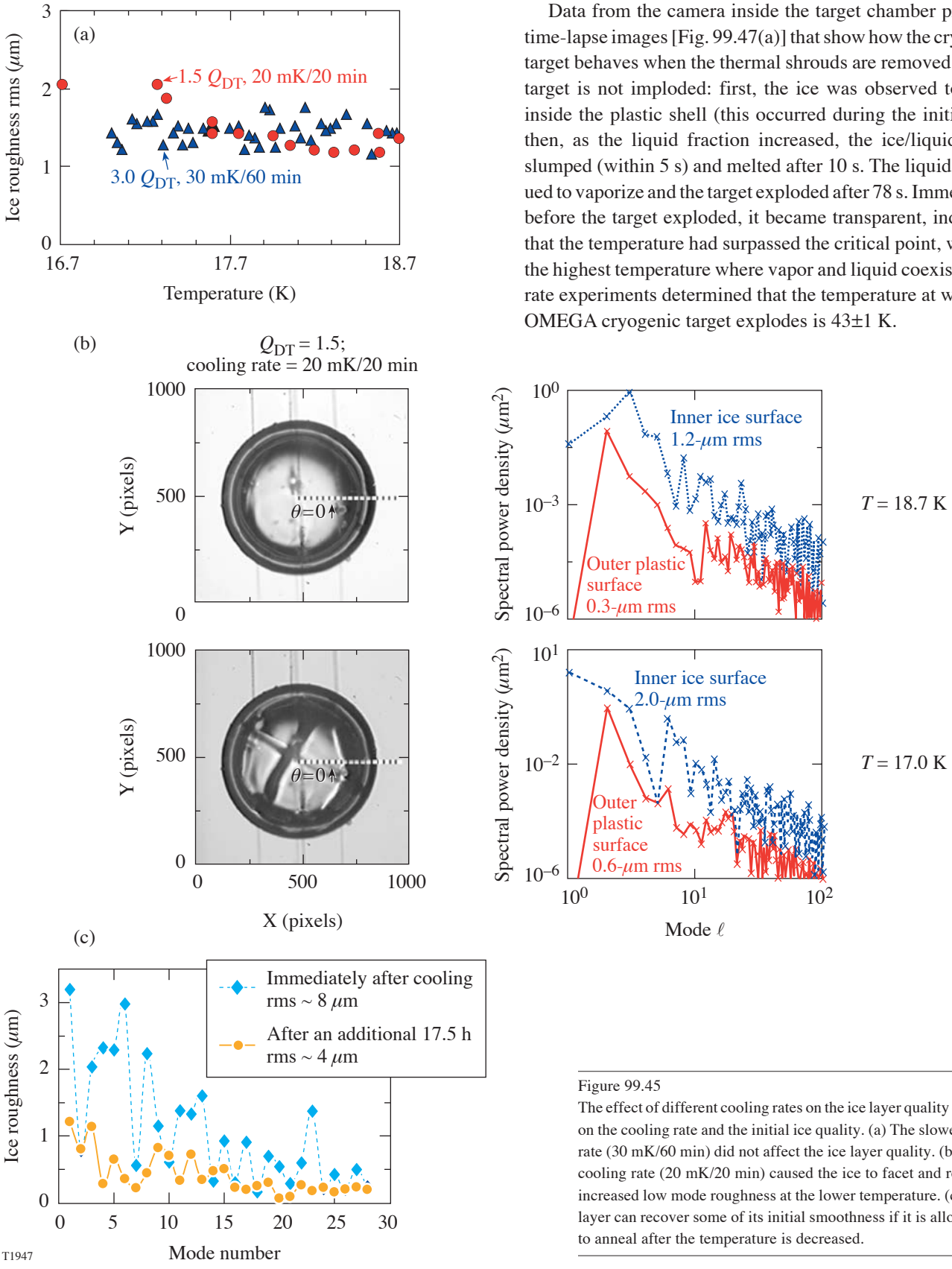

Figure 99.45
The effect of different cooling rates on the ice layer quality depended on the cooling rate and the initial ice quality. (a) The slower cooling rate (30 mK/60 min) did not affect the ice layer quality. (b) The fast cooling rate (20 mK/20 min) caused the ice to facet and resulted in increased low mode roughness at the lower temperature. (c) The ice layer can recover some of its initial smoothness if it is allowed time to anneal after the temperature is decreased.

The target contained 36×10^{-6} g of deuterium, and the combined specific heat of the solid, liquid, and gas required to raise the temperature from 17 K to 43 K was 290 J/g (Ref. 14). Combining this value with the latent heats of fusion and vaporization yielded the total energy required to explode the target, ~0.014 J. These values suggest that the power coupled into the target was 1.7×10^{-4} W, which was ~4% of the estimated 0.0047-W heat flux striking the target. Considering only the time required to melt the ice (10 s), and combining this with the latent heat of fusion for deuterium [50 J/g (Ref. 14)], the calculated heat deposited in the target was approximately 1.8×10^{-4} W.

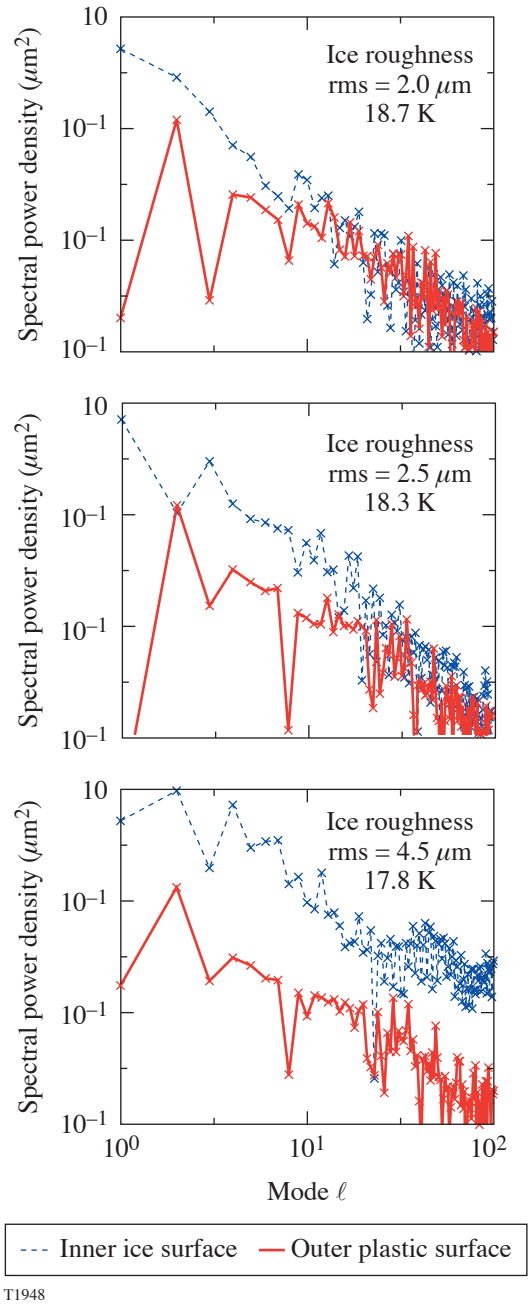

Figure 99.46
The change in the ice power spectrum is shown for a target that roughened when it was cooled.

A detailed thermal model of heat flow through the ice was used to determine how rapidly the temperature of the inner ice surface increased when the target was exposed to ambient radiation. This was done using the computational code FLUENT. For this model, the radiation heat load was coupled into the plastic shell wall alone, as deuterium ice and liquid absorb radiation over such a very limited spectral range (3.1± 0.3 μm) that the power coupled directly into the ice is negligible. The model included the temperature-dependent heat capacity of the solid and the latent heat of fusion for deuterium. The results reported are the time-dependent melt fraction of the ice, the temperature of the inner ice surface, and the heat flux to the inner ice surface. The time-dependent behavior of the ice layer is presented in Fig. 99.47(b) for comparison with the experimental data. In the simulation the ice layer was seen to melt closest to the plastic layer [Fig. 99.48(a)] and then slump on a time scale that was similar to that observed experimentally. This behavior gives confidence that the temperature calculations in the model are relevant.

The sequence of events that occurs once the target is exposed to ambient radiation can be described in more detail using the thermal model as a guide. Initially the ice is at 17 K with a very small radial temperature gradient (<0.1 K). When the shrouds are removed, the plastic absorbs radiation and heats rapidly since the heat capacity of the plastic at this temperature is extremely low (87 J/kg-K). The heat flux from the target to the surroundings is negligible since the target is in vacuum, so all of the heat conducts inward into the ice. The heat flux at the inner ice surface [Fig. 99.48(b)] reaches a peak at ~60 μW after 0.006 s and then decreases to <1 μW within 0.07 s. The behavior follows the radial temperature gradient: after 0.006 s has lapsed, the outer ice surface has reached the triple point (18.72 K) and cannot rise further until the ice is melted; meanwhile, the inner ice surface remained at 17 K. The delay time is due to the thermal diffusivity. Over the next 0.07 s, the outer ice surface remains at the triple point and the inner ice surface approaches the triple-point temperature. Once the inner surface is also at the triple-point temperature, the temperature gradient across the ice layer is negligible and

the heat flux is commensurately low. The time-dependent temperature profile of the inner ice surface is shown in Fig. 99.48(c). As the temperature of the inner ice surface increases, so does the saturated vapor pressure, and the heat flux determines how rapidly ice sublimes to maintain the equilibrium gas pressure. Fortunately, the low heat flux and sizeable latent heat of sublimation [367000 J/kg (Ref. 14)] limits how rapidly the gas density increases in the center of the target [Fig. 99.48(d)]. These data suggest that the gas density will not increase significantly over the sub-0.5 s exposure times when a target at a sub-triple-point temperature is exposed to 300-K radiation.

When a target 1.7 K below the triple point is heated back to the triple-point temperature, the deuterium ice experiences an ~1% volumetric expansion. Should this cause the ice to buckle instead of swelling uniformly, added roughness would be induced on the inner ice surface. Such roughness has not been observed in targets that were imaged in the target chamber, but that may only be because the spatial wavelength and amplitude of the roughness were beyond the resolution of the diagnostic. Ultimately, this effect may determine the allowable target exposure.

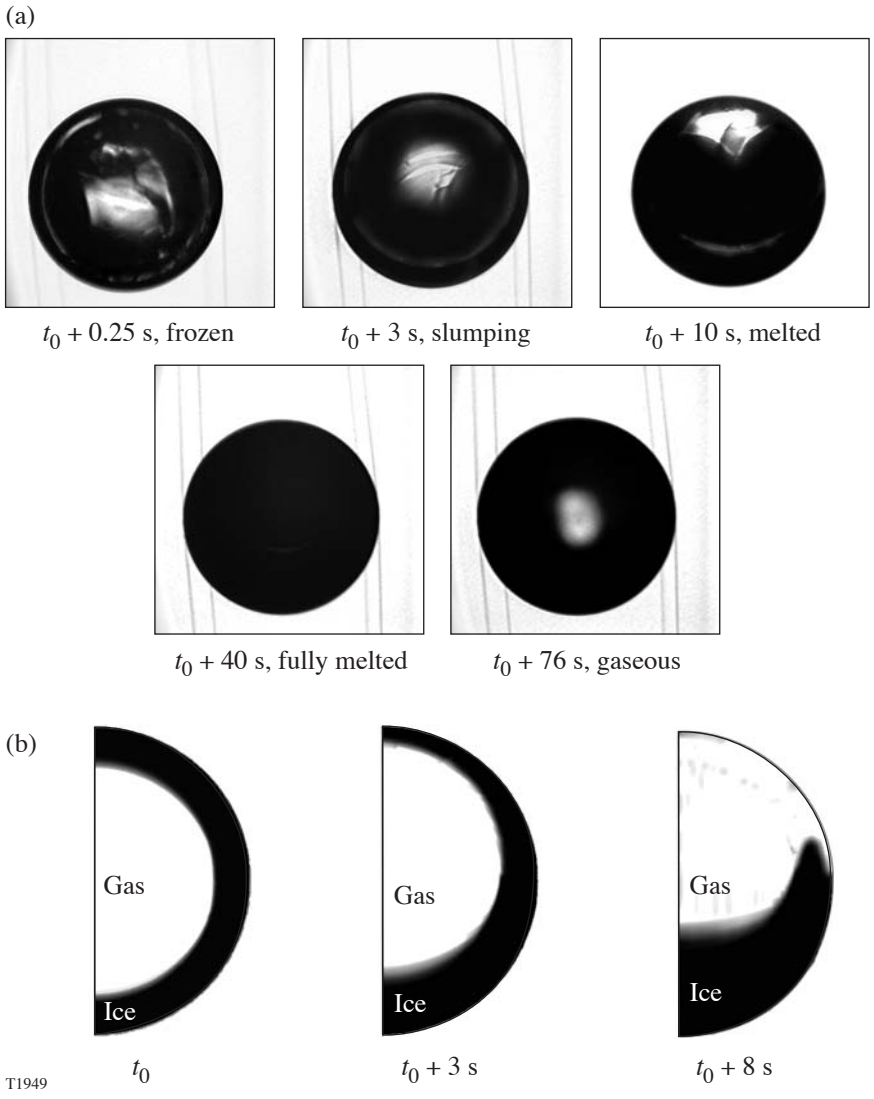

Figure 99.47
(a) Sequence of images showing the ice layer melting and slumping when the thermal shrouds were retracted; (b) calculated response of the ice when the shrouds are removed. The heat absorbed in the plastic caused the target to melt and slump in the same time period that was observed experimentally.

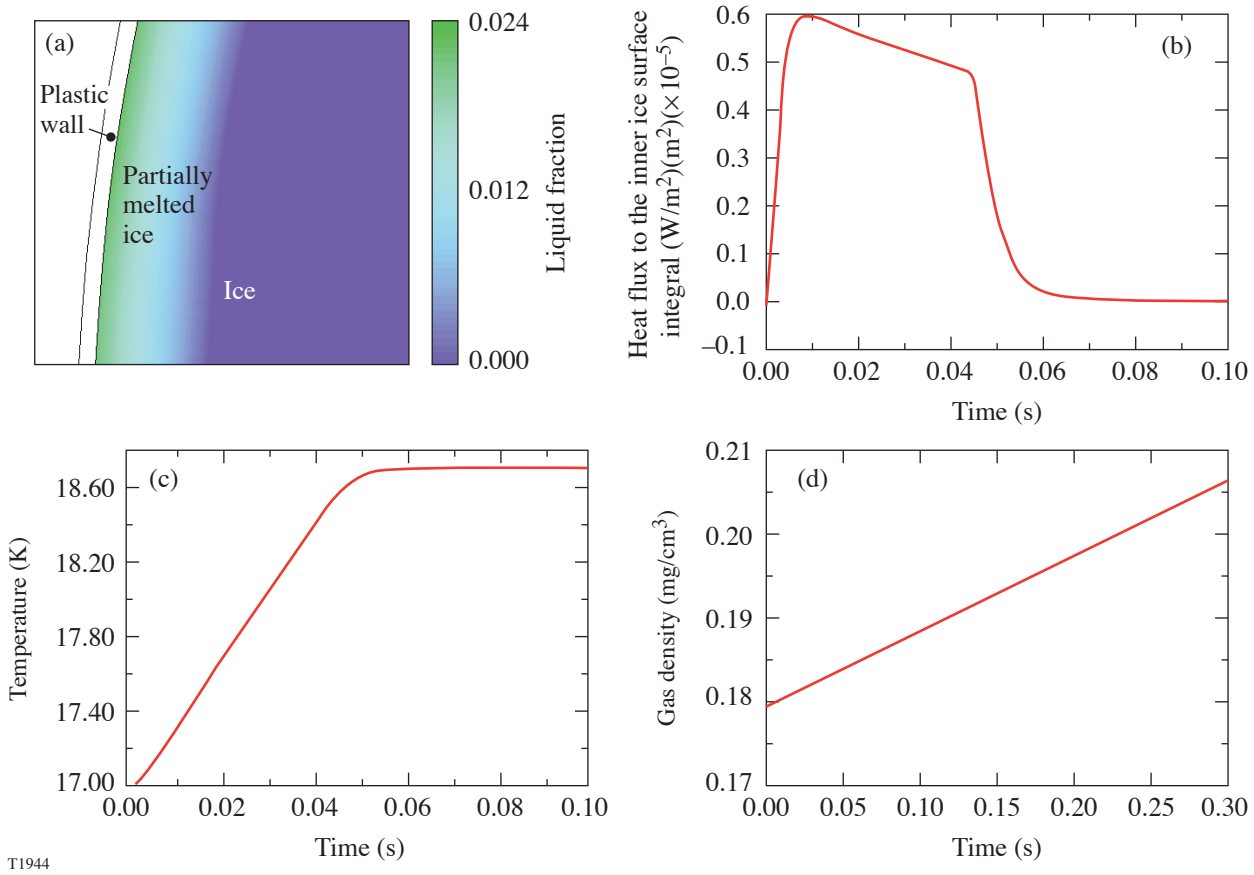

Figure 99.48
Calculated behavior of a cryogenic target when the thermal shroud is removed. (a) Liquid fraction of the outer region of a cryogenic target 0.1 s after being exposed to ambient radiation; (b) calculated heat flux to the inner ice surface; (c) rate of temperature increase of the inner ice surface; (d) density change of the gas in the center of the target.

Summary and Conclusion

High-quality cryogenic targets possessing an ice roughness averaging 1.2 μm for all modes, and for the entire surface, have been demonstrated. These values were achieved by controlling the thermal environment sufficiently to achieve a single initial ice crystal that subsequently grew slowly. A portion of this roughness may be attributable to the nonuniform irradiation of the target caused by the presence of the target-entry hole in the layering sphere. The correlation between this crystal growth phase and the extrinsically controllable parameters (heat flow into and out of the target) has been discussed in terms of the temperature environment within the target. These parameters provide guidelines for a more-complex protocol for controlling the solidification process.

The ice-layering process is controllable: the variability in ice roughness, when the same target is repeatedly layered and melted, is ±0.6 μm. The variability is attributed to intrinsic morphological features within the ice and at the ice/plastic-shell interface, which affects the uniformity of the thermal resistance. The layering process is shown to form a uniformly thick ice layer as evidenced by the ability to form very smooth ice (0.7- to 0.9-μm-rms roughness), albeit over a small cluster set of the 2-D great circles used to completely characterize a target.

It is possible to cool the target to 2 K below the triple point without changing the target's roughness; however, doing so requires a very slow cooling rate. The target's roughness is not

always unaffected even when using the slow cooling rate. When the roughness does change, it is primarily in the lower-order modes. Allowing the target to anneal for an extended period can reverse the roughening, but this does not guarantee that the smoothness will always recover. The variable behavior is attributed to structural changes that the ice undergoes during cooling and densification—changes that affect the radial thermal conductance sufficiently to influence the final ice thickness for which the inner ice surface must be isothermal.

ACKNOWLEDGMENT

This work was supported by the U.S. Department of Energy Office of Inertial Confinement Fusion under Cooperative Agreement No. DE-FC52-92SF19460, the University of Rochester, and the New York State Energy Research and Development Authority. The support of DOE does not constitute an endorsement by DOE of the views expressed in this article.

REFERENCES

1. J. K. Hoffer and L. R. Foreman, Phys. Rev. Lett. **60**, 1310 (1988).
2. G. W. Collins *et al.*, J. Vac. Sci. Technol. A **14**, 2897 (1996).
3. A. Crane and H. P. Gush, Can. J. Phys. **44**, 373 (1966).
4. R. J. Good and G. V. Ferry, in *Advances in Cryogenic Engineering*, edited by K. D. Timmerhaus (Plenum Press, New York, 1963), Vol. 8, pp. 306–310.
5. D. N. Bittner *et al.*, Fusion Technol. **35**, 244 (1999).
6. H. S. Carslaw and J. C. Jaeger, *Conduction of Heat in Solids*, 2nd ed. (Clarendon Press, Oxford, 1959).
7. E. H. Kennard, *Kinetic Theory of Gases, with an Introduction to Statistical Mechanics*, 1st ed. (McGraw-Hill, New York, 1938).
8. G. K. White, *Experimental Techniques in Low-Temperature Physics*, 2nd ed., Monographs on the Physics and Chemistry of Materials (Clarendon Press, Oxford, 1968).
9. D. N. Bol'shutkin, Yu. E. Stetsenko, and L. A. Alekseeva, Sov. Phys.-Solid State **12**, 119 (1970).
10. M. Wozniak, *2003 Summer Research Program for High School Juniors at the University of Rochester's Laboratory for Laser Energetics*, University of Rochester, Rochester, NY, Laboratory for Laser Energetics Report No. 332, NTIS document No. DOE/SF/19460-526 (2004). Copies may be obtained from the National Technical Information Service, Springfield, VA 22161.
11. Fluent USA Inc., Lebanon, NH 03766.
12. R. W. Powers, R. W. Mattox, and H. L. Johnston, J. Am. Chem. Soc. **76**, 5972 (1954).
13. D. S. Metzger and J. R. Gaines, Phys. Rev. **147**, 644 (1966).
14. P. C. Souers, *Hydrogen Properties for Fusion Energy* (University of California Press, Berkeley, 1986).